Acta Crystallographica Section D
Biological Crystallography
ISSN 0907-4449

The atomic resolution structure of bucandin, a novel toxin isolated from the Malayan krait, determined by direct methods

Peter Kuhn,[a]† Ashley M. Deacon,[a]† Silviana Comoso,[b] G. Rajaseger,[c] R. Manjunatha Kini,[c] Isabel Usón[d] and Prasanna R. Kolatkar[b]*

[a]Stanford Synchrotron Radiation Laboratory, SLAC, PO Box 4349, MS69, Stanford University, Stanford, CA 94309, USA, [b]Institute of Molecular and Cell Biology–Bioinformatics Centre, 30 Medical Drive, Singapore 117609, Singapore, [c]Bioscience Centre, Faculty of Science, NUS, Singapore 119260, Singapore, and [d]Institute of Inorganic Chemistry, Tammannstrasse 4, 37077 Göttingen, Germany

† PK and AMD contributed equally to this work.

Correspondence e-mail: kolatkar@bic.nus.edu.sg

Received 19 May 2000
Accepted 18 August 2000

PDB Reference: bucandin, 1f94.

Bucandin is a novel presynaptic neurotoxin isolated from *Bungarus candidus* (Malayan krait). It has the unique property of enhancing presynaptic acetylcholine release and represents a family of three-finger toxins with an additional disulfide in the first loop. There are no existing structures from this sub-category of three-finger toxins. The X-ray crystal structure of bucandin has been determined by the *Shake-and-Bake* direct-methods procedure. The resulting electron-density maps were of outstanding quality and allowed the automated tracing of 61 of the 63 amino-acid residues, including their side chains, and the placement of 48 solvent molecules. The 0.97 Å resolution full-matrix least-squares refinement converged to a crystallographic R factor of 12.4% and the final model contains 118 solvent molecules. This is the highest resolution structure of any member of the three-finger toxin family and thus it can serve as the best model for other members of the family. Furthermore, the structure of this novel toxin will help in understanding its unique ability to enhance acetylcholine release. The unique structure resulting from the fifth disulfide bond residing in the first loop improves the understanding of other toxins with a similar arrangement of disulfide bonds.

1. Introduction

Snake-venom toxins are used as research tools and play an important role in the development of therapeutic agents. These toxins belong to a small number of protein superfamilies. Among these, the three-finger toxin family is a well characterized group of non-enzymatic polypeptides. They exhibit diverse pharmacological effects. Members of this family include postsynaptic neurotoxins, cardiotoxins and cytotoxins, fasciculins, platelet-aggregation inhibitors and specific ion-channel blockers. The three-dimensional structures of several three-finger toxins have been determined to date. These include cardiotoxin (Rees *et al.*, 1990), fasciculin (Le Du *et al.*, 1992), erabutoxin a and b (Corfield *et al.*, 1989; Smith *et al.*, 1988), α- and κ-bungarotoxin (Love & Stroud, 1986; Dewan *et al.*, 1994) and α-cobratoxin (Betzel *et al.*, 1991). Despite the functional diversity, they all share similar protein-folding characteristics: three β-stranded loops extending from a central core, containing four conserved disulfide bonds. Some members, such as the long-chain neurotoxins and κ-bungarotoxins, have an additional disulfide bond in loop 2 which serves to lock its extremity (Menez *et al.*, 1992; Rees & Bilwes, 1993; Menez, 1993, 1998).

Bucandin consists of 63 amino-acid residues and a comparison (Fig. 1) of toxin sequences shows that it is most similar to the toxin S6C4 isolated from *Dendroaspis j.*

kaimosae (68.8% identity). A sequence identity of 30–40% is found when comparing bucandin with other three-finger toxins. This high degree of sequence homology results mostly from the conserved disulfide bonds (which constitute 10–15% of the sequence identity) and some additional residues forming the core β-sheet lattice in which the functional residues are most likely to be located.

Bucandin is a novel presynaptic toxin. Most presynaptic toxins are either phospholipase A_2 enzymes or contain these enzymes as an integral part of the neurotoxin complex. These toxins inhibit the release of acetylcholine (ACh). However, the mechanisms of inhibition vary and have not yet been completely delineated. Dendrotoxins, in contrast, bind to potassium channels and thus induce the release of ACh (Rees & Bilwes, 1993; Menez, 1993). Atrotoxin is a presynaptic neurotoxin isolated from the venom of the black widow spider *Latrodectus tredecimguttatus* (Menez, 1993). It exerts toxic effects in the vertebrate central nervous system by increasing the internal concentration of calcium ions and thereby depolarizing neurones and also by stimulating uncontrolled exocytosis of neurotransmitters from nerve terminals. Bucandin is the first toxin that enhances the release of ACh. Therefore, it is important to understand the structural features of this novel toxin.

In this paper, we report the identification, characterization, sequencing and structure determination of a new snake-venom toxin, bucandin. The structure of this toxin will help in understanding its unique ability to enhance acetylcholine release.

2. Materials and methods

2.1. Isolation and purification

Bucandin was purified to homogeneity by a two-step protocol as follows. The *B. candidus* venom was isolated from its native source by separating the crude venom into seven fractions on a Superdex 30 gel-filtration column. The last protein fraction was eluted after the salt volume of the column; the proteins in this peak were further fractionated on a reversed-phase HPLC column. The major protein peak was named bucandin. It was shown to be homogeneous by electrospray ionization mass spectrometry. Bucandin has a molecular mass of 7275.43 $\pm$ 0.32 Da and represents about 2–3% of the crude venom. Amino-terminal sequencing of the native and pyridylethylated protein (Cavins & Friedman, 1970; Kini & Evans, 1989) was performed by automated Edman degradation using a Perkin–Elmer Applied Biosystems 494 pulsed liquid-phase protein sequencer (Procise) with an on-line 785A PTH amino-acid analyzer. This allowed the precise identification of all amino-acid residues and revealed the complete sequence of both native (blank cycles where Cys residues are found) and pyridylethylated bucandin samples. Bucandin consists of 63 amino-acid residues including ten cysteine residues. The calculated mass is 7275.24 Da.

2.2. Crystallization

Crystallization conditions were established using the sparse-matrix method. The bucandin crystals were grown by vapor diffusion from hanging drops containing a 1:1(v/v) ratio of protein stock solution (3 µl, 10 mg ml^{-1}) to well solution (3 µl) at room temperature. The well solution contained 30% 2-propanol, 0.1 *M* Tris–HCl pH 8.5 and 0.2 *M* ammonium acetate. Crystals belong to the space group *C*2, with unit-cell parameters a = 76.97, b = 22.52, c = 32.60 Å, $\alpha = \gamma = 90$, $\beta = 100.23^\circ$, and contain one molecule in the asymmetric unit.

2.3. X-ray data collection and processing

Following the addition of 2 µl of 50% glycerol as a cryoprotectant to the crystallization drop, a single crystal of bucandin with approximate dimensions 20 × 20 × 250 µm was rapidly immersed into a stream of evaporated liquid nitrogen. Diffraction data were collected at SSRL BL9-1 at a temperature of 183 K maintained by a cold nitrogen-gas stream (Bellamy *et al.*, 1994). A MAR345 imaging-plate detector was mounted on the beamline, which was operated at a wavelength of 0.98 Å. A total of 33 363 reflections were measured in the resolution range 32.0–0.97 Å. The data were integrated and scaled using *MOSFLM* (Leslie, 1991) and *SCALA* (Evans, 1993) and resulted in a 99.5% complete data set, with a multiplicity of 3.7 and an $R_{\rm merge}$ of 5.5% (Table 1).

2.4. Structure determination by direct methods

The structure of bucandin was solved by direct methods. Both the *SnB* v2.0 (Weeks & Miller, 1999) and the *SHELXD* (Sheldrick, 1998; Usón & Sheldrick, 1999)

Protein	Venom	1	10	20	30
Bucandin	*Bungarus candidus*	M E C Y R C G V S G C		H L K I T C S A E E T F C Y K W L N K I	
S_6C_4	*Dendroaspis j. kaimosae*	L E C Y R C G V S G C		H L R T T C S A K E K F C A K Q H N R I	
Candoxin	*Bungarus candidus*	M K C K I C N F D T C R A G E L K V C A S G E K Y C F K E S W R E			
Long neurotoxin homolog	*Bungarus multicinctus*	M K C K I C H F D T C R A G E L K V C A S G E K Y C F K E S W R E			
CM-9a	*Naja naja kauthia*	L R C L N C P E M F C		G K F Q I C R N G E K I C F K K L H Q R	
CM-10	*Naja nivea*	L R C L N C P E V F C		R N F H T C R N G E K I C F K R F D Q R	
CM-11	*Naja haje haje*	L T C F I C P E K Y C		N K V H T C R N G E N Q C F K R F N E R	
CM-13b	*Naja haje annulifera*	L T C F N C P E V Y C		N R F H T C R N G E K I C F K R F N E R	
S_4C_{11}	*Naja melanoleuca*	L T C L I C P E K Y C		N K V H T C R N G E N I C F K R F Y E G	

Protein	40	50	60	Homology (%)
Bucandin	S N E R W L G C A K T C T E I D T W N V Y N K C C T T N L C N T			----------
S_6C_4	S T L W W H G C V E T C T E D E T W K F Y R K C C T T N L C N I			68.8 (75.0)
Candoxin	A R G T R I E R G C A A T C P K G S V Y G L Y V L C C T T D D C N			29.8 (38.8)
Long neurotoxin homolog	A R G T R I E R G C A A T C P K G S V Y G L Y V L C C T T D D C N			29.8 (38.8)
CM-9a	R P L S R Y I R G C A D T C P V G Y P K E M I E C C S T D K C N R			28.8 (37.9)
CM-10	K L L G K R Y T R G C A V T C P V A K P R E I V E C C S T D G C N R			28.8 (37.9)
CM-11	K L L G K R Y T R G C A A T C P E A K P R E I V E C C T T D R C N K			33.3 (40.9)
CM-13b	K L L G K R Y P T G C A A T C P V A K P R E I V E C C S T D K C N H			30.3 (39.4)
S_4C_{11}	N L L G K R Y P R G C A A T C P E A K P R E I V E C C S T D K C N H			30.3 (37.9)

Figure 1
Sequence comparison of bucandin with other toxins. Percentage identity and percentage similarity (in parentheses) are given after the sequences.

Table 1
Summary of X-ray diffraction data.

The data were collected at SSRL beamline 9.1 using a MAR345 detector.

Data type	Slow pass	Quick pass	Total
Wavelength (Å)	0.98	0.98	0.98
Resolution range (Å)	3.0–0.97	32.0–2.0	32.0–0.97
No. of observations	105047	14310	119818
No. unique	31699	4308	33363
Completeness (%)			
Overall	97.2	98.9	99.5
Last shell†	94.7	98.9	94.7
R_{sym}‡ (%)			
Overall	8.6	3.7	5.5
1.11–1.08 Å	30.0		30.0
1.08–1.05 Å	38.4		38.4
Last shell†	66.4	6.1	66.4
Average $I/\sigma(I)$			
Overall	6.0	14.1	5.7
Last shell†	1.1	10.7	1.1

† Last resolution shells: slow pass, 1.00–0.97 Å; quick pass, 2.25–2.00 Å. ‡ $R_{sym} = \sum_i |I_i - \langle I \rangle| \sum \langle I \rangle$, where $\langle I \rangle$ is the mean intensity of the N reflections.

Table 2
Phasing and refinement statistics and model quality.

Phasing	
Minimal function of solution	0.452
Correlation coefficient	0.78
Refinement	
Resolution (Å)	32.0–0.97
Number of atoms (average B value in Å^2)	634 (25.6)
Protein	516 (21.9)
Water	118 (41.6)
Number of refinement parameters	5705
Number of refinement restraints	6823
R factor (No. reflections included)	12.37 (33339)
R_{free} (No. reflections included)	16.00 (1201)
R.m.s. deviation from ideal geometry	
Bonds (Å)	0.017
Angles (°)	2.26

implementations of the *Shake-and-Bake* dual-space direct-methods procedure (Weeks *et al.*, 1994) were used to derive independent *ab initio* solutions from the X-ray diffraction data.

For the *SnB* v2.0 structure determination, normalized structure-factor magnitudes (E values) were calculated for all diffraction data in the resolution range 32.0–1.1 Å using the programs *LEVY* and *EVAL* (Blessing *et al.*, 1996), which are built into the *SnB* v2.0 program. The 5000 largest of these E values were then used to generate 50 000 triplet invariants. A total of 542 random trials were processed and each trial was subjected to 500 cycles of real-space (peak-picking) and reciprocal-space (parameter-shift) refinement. The final minimal functions of these trials were clearly bimodal (Hauptman, 1991), where the minimal function of one of these trials ($R_{min} = 0.452$) was significantly lower than the rest of the trials ($R_{min} = 0.475$–0.502).

The *SHELXD* program calculates its own E values. Data were cut to a resolution of 1.05 Å, as the average $I/\sigma(I)$ fell below 2.0 beyond this resolution. Starting from a trial set of random atoms, phases were refined by the tangent formula (Karle, 1968) in reciprocal space, alternating with the selection of the 150 highest peaks in an E map calculated using the strongest E magnitudes (3452 E values > 1.4). An average of 98.8 triplets were used for each phase. One-third of these potential atoms were then eliminated at random. After 150 such real-space/reciprocal-space iterations, possible solutions were screened by checking the value of the correlation coefficient (CC) between observed and calculated normalized structure-factor amplitudes based on all data (Fujinaga & Read, 1987). Partial solutions with a CC of above 40% invariably led to a full structure solution. These partial solutions were expanded by eight cycles of progressively incorporating more atoms coupled with peak-list optimization (Sheldrick & Gould, 1995). Peaks were eliminated from bottom to top whenever this led to an improvement in the CC. These full solutions were characterized by a final CC of greater than 78%. After 1000 random trials, the structure had been solved five times, each leading to the correct location of 500 atoms. The presence of five disulfide bridges accelerated the structure solution because it enabled a relatively small subset of atoms (~100) to be located within the internal loop using only the strongest data.

Bucandin is the largest structure determined *de novo* by the *SnB* v2.0 program, although the program has been used on some larger test cases such as triclinic lysozyme (Deacon *et al.*, 1998); it is also one of the largest structures determined by *SHELXD*, although two larger all light-atom structures (V-amylose and mersacidin) with 624 atoms plus 147 solvent sites and 750 atoms plus 100 solvent sites, respectively, have been solved recently (Gessler *et al.*, 1999; Schneider *et al.*, 2000).

The resulting electron-density maps were of excellent quality (Figs. 2*a* and 2*b*). In principle, it was possible to build an initial model by selecting individual peaks from one solution or by subjecting a σ_A map (Read *et al.*, 1986) obtained after B-value refinement of an unexpurgated solution (Usón *et al.*, 1999) to standard protein map-tracing methods. However, in our case the phases output from the *SnB* v2.0 solution were input directly into the program *wARP* (Perrakis *et al.*, 1999), which proceeded quickly from an initial trace of 48 residues broken into four discrete chains to a final trace, after ten cycles, of 61 residues in a single polypeptide chain. Subsequent automated side-chain docking against the known amino-acid sequence allowed the correct placement of 70% of the side-chain groups. An additional two residues at the C- and N-termini and the remainder of the side chains were fitted manually using the *XtalView* suite of programs (McRee, 1992). The complete *SnB* solution and automated tracing and building were accomplished within 24 h.

2.5. Structure refinement

The subsequent refinement of the initial model against the diffraction data was carried out with *SHELXL* (Sheldrick & Schneider, 1997). The data-to-parameter ratio of 5.8 allowed the refinement of anisotropic temperature factors, as judged by a drop of 4.97% in the R_{free} (based on 5% randomly

selected reflections which were omitted from all refinement cycles except for the final round). The standard conjugate-gradient least-squares refinement converged after two rounds of manual refitting to a crystallographic R factor of 13.2% ($R_{\rm free}$ = 15.8%) for all data in the resolution range 32.0–0.97 Å. This was followed by full-matrix least-squares refinement in which the model, containing H atoms, was refined against all data. This converged to an R factor of 12.4%. The final model contained all 63 amino-acid residues, of which three show two distinct conformations, and 118 solvent molecules. The side chain for Glu20 was disordered and could not be interpreted from the electron-density maps and was omitted from the final model (truncated to the CB position). A final round of full-matrix least-squares refinement in *SHELXL* allowed the estimation of standard deviations on the atomic coordinates from the inversion of the least-squares matrix. This indicated an average coordinate error of about 0.029 Å. The final model exhibited good stereochemical geometry (Table 2). All stereochemical parameters are within the expected margins and the Ramachandran plot (Ramachandran *et al.*, 1974) shows 86.2% of residues in the most favoured and 13.8% in the additional allowed region, with none in the generously allowed or disallowed region as defined in *PROCHECK* (Laskowski *et al.*, 1993). Electrostatic potentials for bucandin were calculated with *GRASP* (Nicholls *et al.*, 1991).

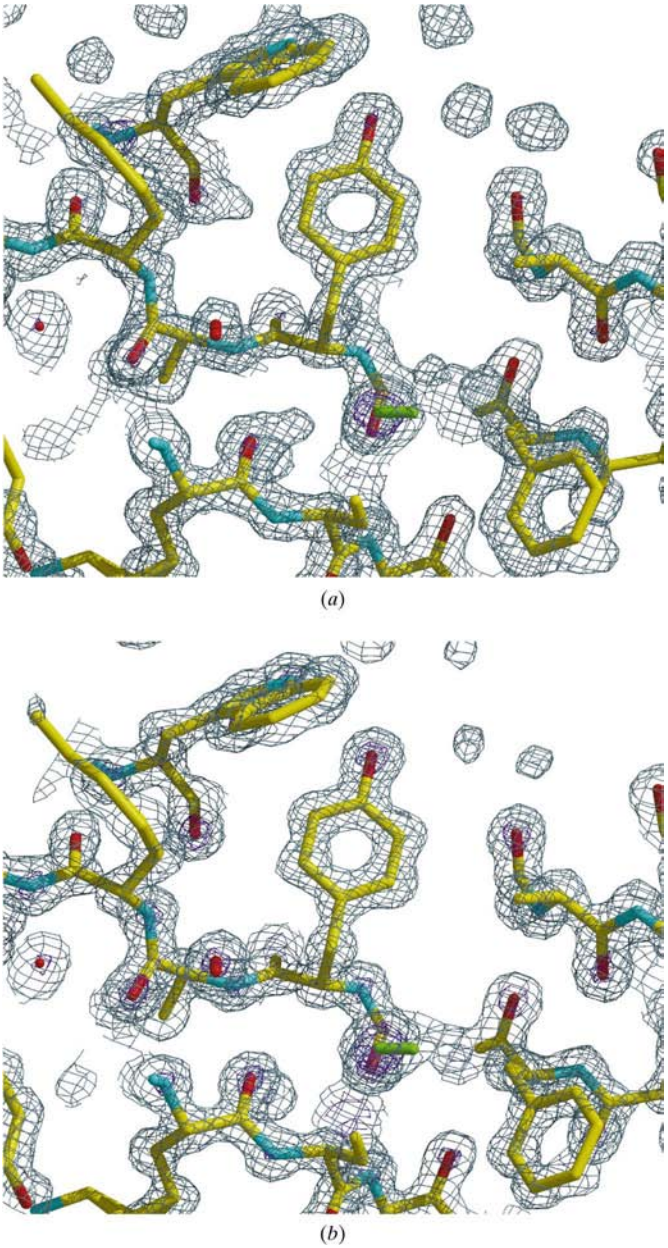

Figure 2
Electron-density maps obtained from (*a*) *SnB* v2.0, (*b*) the final refined model ($2F_o - F_c$). The maps are contoured at 1.0σ (gray) and 5.0σ (magenta).

3. Results and discussion

3.1. Description of the overall structure

The structure of bucandin comprises two antiparallel β-sheets. The first sheet contains two strands: β1 (residues 1–5) and β2 (residues 13–17) from loop 1, while the other contains four strands: β3 (residues 23–28), β4 (residues 35–39), β5 (residues 45–48) and β6 (residues 51–57) from loops 2 and 3 (Figs. 3*a* and 3*b*). This is the first known toxin structure to have an additional fourth strand (β5) in the main β-sheet. The formation of this fourth strand causes the bucandin molecule to be extremely flat, with dimensions of approximately 36 × 24 × 12 Å. Bucandin contains five disulfide bonds, of which four (Cys3—Cys24, Cys17—Cys39, Cys43—Cys55 and Cys56—Cys61) occur in the central core of the molecule, similar to many other three-finger toxins. As expected, the fifth disulfide (Cys6—Cys11) is located in the first loop, where it disrupts the β-sheet and stabilizes an unusual kink, causing the β-strands to turn nearly 90° with respect to the rest of the molecule. There are exposed hydrophobic residues on both faces of the molecule. One face (face *A*) has three tryptophans all facing out from the molecule (Fig. 4*a*). This face also has two small patches of negative and two small patches of positive charge. The opposite face (face *B*) has a large patch of positive charge located centrally within the molecule (Fig. 4*b*). Indeed, a dipole vector was calculated which demonstrated the large differences in charge between the two faces of the molecule (Figs. 4*a* and 4*b*). The crystal packing diagram does not show any obvious multimer conformations.

3.2. Comparisons with other toxins

Most three-finger toxins exhibit their pharmacological effects through interaction with specific receptors. Erabutoxin, α-bungarotoxin and cobratoxin all bind to the postsynaptic ACh receptor (AChR) of the neuromuscular junction (Rees & Bilwes, 1993). Another member of the three-finger toxin family, κ-neurotoxin, acts on postsynaptic AChRs of the central nervous system rather than the peripheral neuromuscular junctions (Menez *et al.*, 1992), while cardiotoxins have a multitude of effects with poorly understood mechanisms. The platelet-aggregation inhibitor dendroaspin binds to

fibrinogen-receptor glycoprotein IIb–IIIa complex and disrupts its interaction with fibrinogen (Sutcliffe *et al.*, 1994), whereas calciseptine binds to L-type calcium channel and blocks the calcium current (Menez, 1993). The mechanism of the presynaptic action of bucandin is unknown; however, its structure does suggest some possibilities. The unusual kink in the first loop could be useful in isolating this portion of the structure and preventing any interference with the charges in the rest of the molecule or it could also function to rigidify the molecule and thereby facilitate some specific interactions. This is unlike other α-neurotoxins, which have loops that are in closer proximity to the rest of the molecule (Fig. 5). The *A* side with its unique tryptophan array may be involved in interacting with an unidentified presynaptic receptor/acceptor protein, while the electrostatic charges could provide some initial specific coulombic interactions, similar to toxins which target AChR. Alternatively, the hydrophobic patch on side *A*

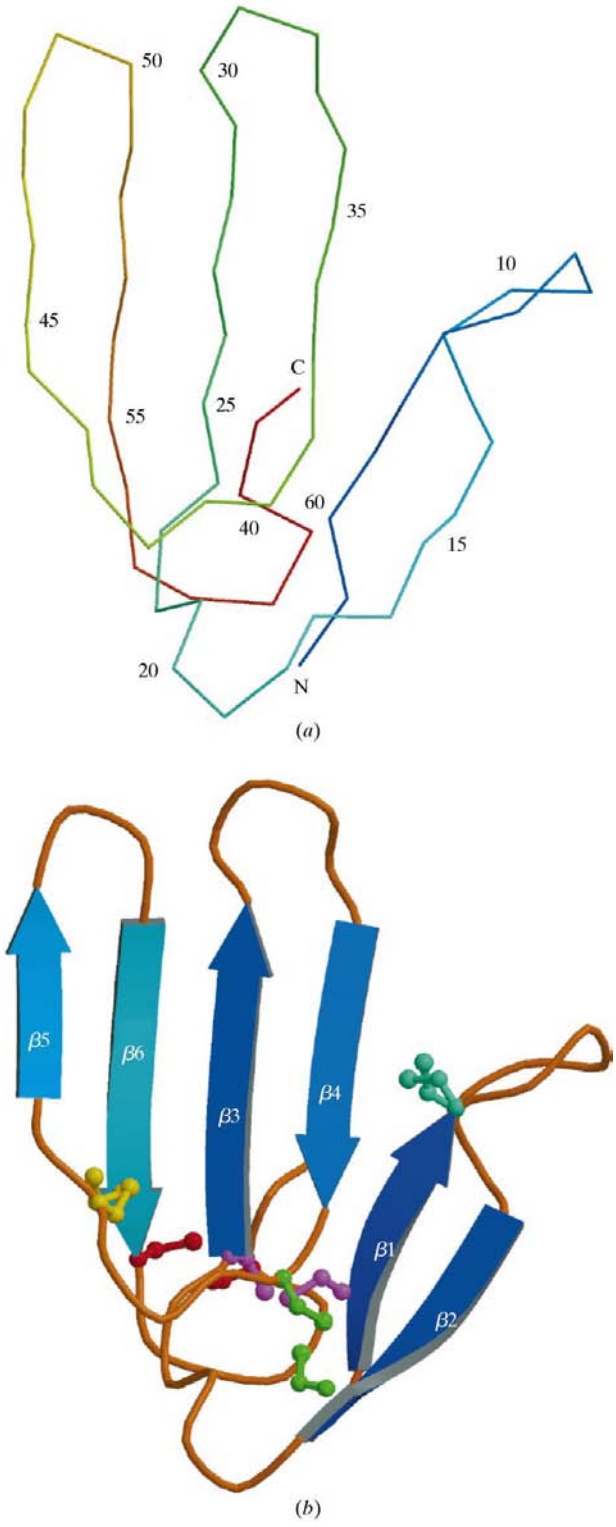

Figure 3
(*a*) Numbered C^{α} trace, color coded from the N-terminus (blue) to the C-terminus (red). (*b*) Ribbon diagram of bucandin: the β-sheets are labelled and the cysteine residues contributing to each disulfide are colored uniquely.

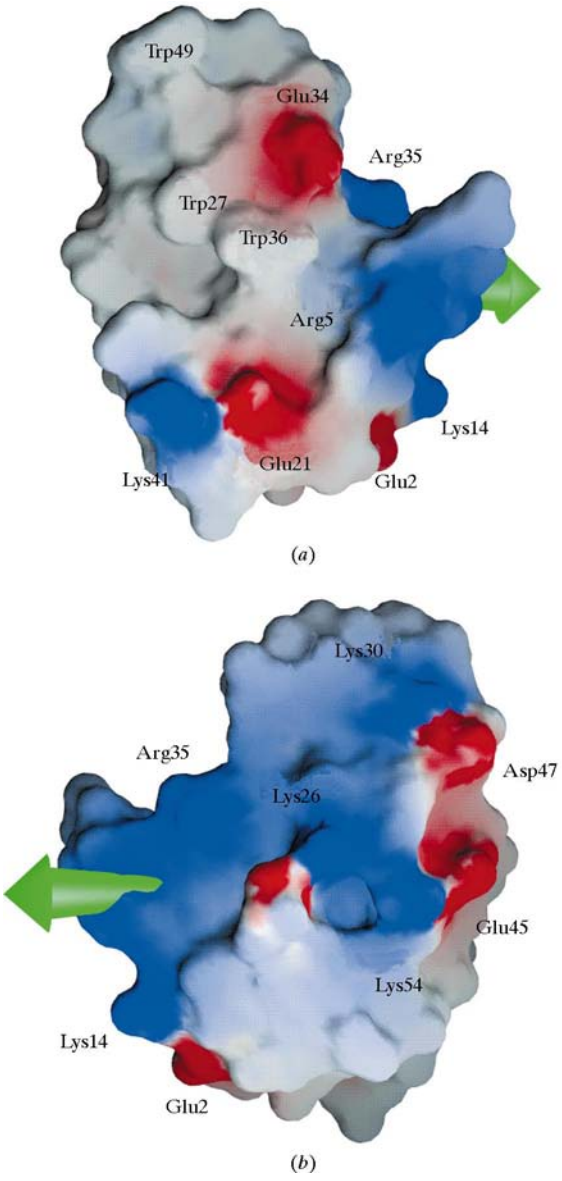

Figure 4
A surface plot showing the electrostatic potential of bucandin. Selected residues which could have functional relevance are marked. Panels (*a*) and (*b*) show the two faces of the flat bucandin molecule. The green arrow represents the dipole moment calculated for bucandin.

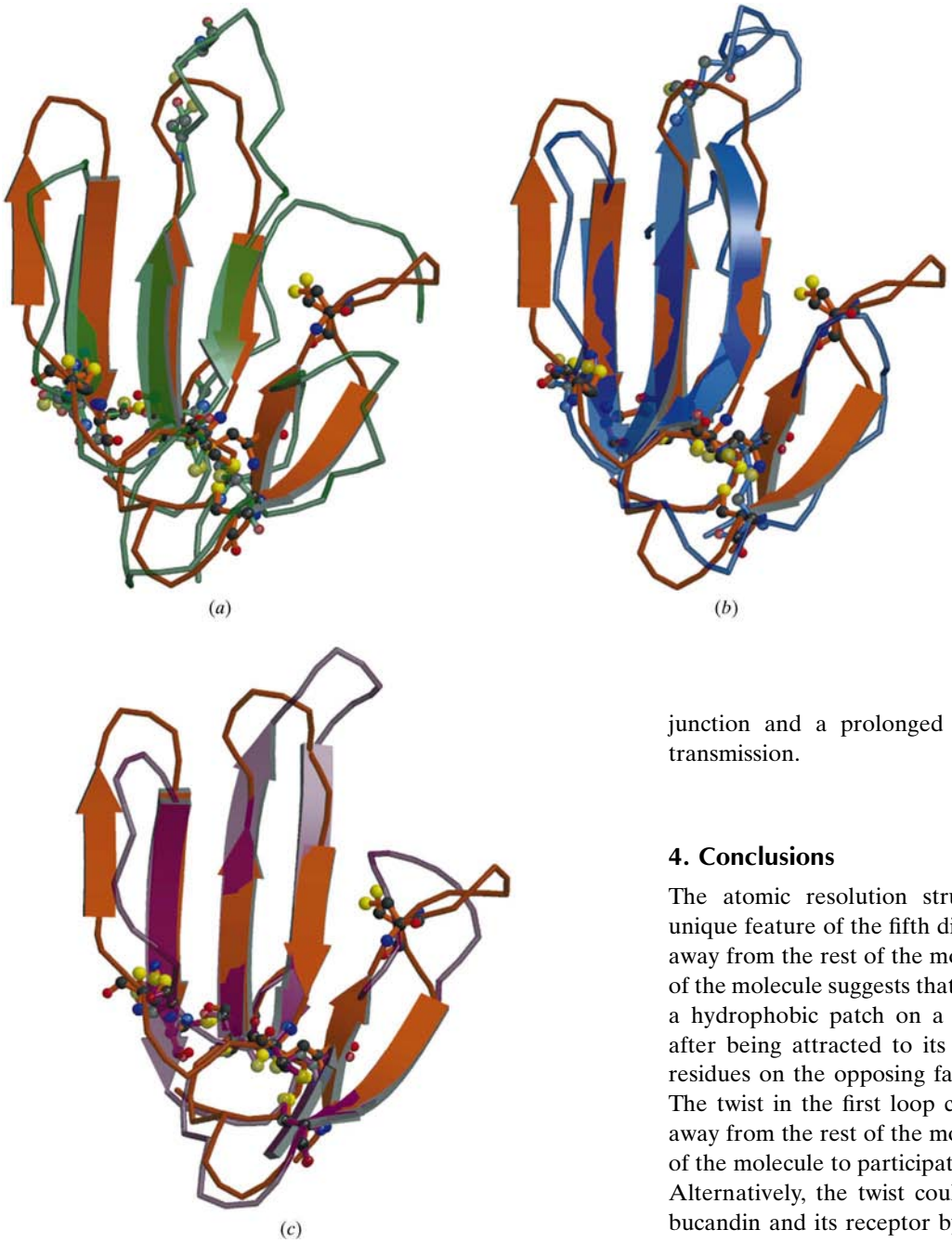

Figure 5
Structural comparisons of (*a*) bucandin with cobratoxin (1ctx), (*b*) erabutoxin (3ebx) and (*c*) bungarotoxin (2abx). Bucandin is colored orange in each figure. The similarity of structures is apparent, as well as the significant differences within the loop regions. The nearly 90° turn of the first loop of bucandin relative to the rest of the molecule shows a significant difference compared with other toxins. The presence of a fourth β-strand in bucandin is clearly seen on the left of the molecule.

and a positively charged *B* side could facilitate a function of general membrane disruption. The dual nature of the molecule could allow penetration and association with lipid bilayers of membranes, as in snake-venom cardiotoxins and scorpion toxins. However, the specificity of binding makes this general membrane-disruption hypothesis less likely than bucandin acting as a neurotoxin upon a specific receptor.

Further studies are essential to identify the precise interaction site and understand its structure–function relationships. Such studies will help in developing therapeutic agents against myasthenia gravis, where even though the ACh is released normally, its effect on the post-synaptic membrane is reduced owing to a decrease in the number of AchRs (Drachman, 1994). Bucandin may provide a better alternative to acetylcholinesterase inhibitors, leading to substantial ACh accumulation at the neuromuscular junction and a prolonged enhancement of neuromuscular transmission.

4. Conclusions

The atomic resolution structure of bucandin reveals the unique feature of the fifth disulfide, which twists the first loop away from the rest of the molecule. The highly dipolar nature of the molecule suggests that the molecule may be attaching to a hydrophobic patch on a complementary receptor surface after being attracted to its binding location by the charged residues on the opposing face of the flat bucandin molecule. The twist in the first loop could also serve to help isolate it away from the rest of the molecule and thereby allow the rest of the molecule to participate in interactions with its receptor. Alternatively, the twist could facilitate interactions between bucandin and its receptor by creating a more rigid molecule, allowing more specific interactions. Further biochemical studies of bucandin and structural studies of other three-finger toxins with similar disulfide arrangements will allow a better correlation between this unique structural property and the molecular function.

We thank Anand R. Kolatkar and Mike Soltis for assistance with data collection and analysis and Anastassis Perrakis for a prerelease of *wARP* to allow for direct sequence alignment of the structure. This work is in part based upon research conducted at the Stanford Synchrotron Radiation Laboratory (SSRL), which is funded by the Department of Energy (BES, BER) and the National Institutes of Health (NCRR, NIGMS). The work was also supported in part by the Economic Development Board of Singapore.

References

Bellamy, H., Phizackerley, R. P., Soltis, S. M. & Hope, H. (1994). *J. Appl. Cryst.* **27**, 967–970.

Betzel, C., Lange, G., Pal, G. P., Wilson, K. S., Maelicke, A. & Saenger, W. (1991). *J. Biol. Chem.* **266**(32), 21530–21536.

Blessing, R. H., Guo, D. Y. & Langs, D. A. (1996). *Acta Cryst.* D**52**, 257–266.

Cavins, J. F. & Friedman, M. (1970). *Anal. Biochem.* **35**(2), 489–493.

Corfield, P. W. R., Lee, T. J. & Low, B. W. (1989). *J. Biol. Chem.* **264**(16), 9239–9242.

Deacon, A. M., Weeks, C. M., Miller, R. & Ealick, S. E. (1998). *Proc. Natl Acad. Sci. USA*, **95**, 9284–9289.

Dewan, J. C., Grant, G. A. & Sacchettini, J. C. (1994). *Biochemistry*, **33**(44), 13147–13154.

Drachman, D. (1994). *N. Engl. J. Med.* **330**(25), 1797–1810.

Evans, P. R. (1993). *Proceedings of the CCP4 Study Weekend. Data Collection and Processing*, edited by L. Sawyer, N. Isaacs & S. Bailey, pp. 114–122. Warrington: Daresbury Laboratory.

Fujinaga, M. & Read, R. J. (1987). *J. Appl. Cryst.* **20**, 517–521.

Gessler, K., Usón, I., Takaha, T., Krauss, N., Smith, S. M., Okada, S., Sheldrick, G. M. & Saenger, W. (1999). *Proc. Natl Acad. Sci. USA*, **96**, 4246–4251.

Hauptman, H. A. (1991). *Crystallographic Computing 5: From Chemistry to Biology*, edited by D. Moras, A. D. Podjarny & J. C. Thierry, pp. 324–332. Oxford University Press.

Karle, J. (1968). *Acta Cryst.* B**24**, 182–186.

Kini, R. M. & Evans, H. J. (1989). *Biochemistry*, **28**(23), 9209–9215.

Laskowski, R. A., McArthur, M. W., Moss, D. S. & Thornton, J. M. (1993). *J. Appl. Cryst.* **26**, 283–291.

Le Du, M. H., Marchot, P., Bougis, P. E. & Fontecilla-Camps, J. C. (1992). *J. Biol. Chem.* **267**(31), 22122–22130.

Leslie, A. G. W. (1991). *Crystallographic Computing 5: From Chemistry to Biology*, edited by D. Moras, A. D. Podjarny & J. C. Thierry, pp. 50–61. Oxford University Press.

Love, R. A. & Stroud, R. M. (1986). *Protein Eng.* **1**(1), 37–46.

McRee, D. E. (1992). *J. Mol. Graph.* **10**, 44–46.

Menez, A. (1993). *Pour la Science*, **190**, 34–40.

Menez, A. (1998). *Toxicon*, **36**(11), 1557–1572.

Menez, A., Bontems, F., Roumestand, C., Gilquin, B. & Toma, F. (1992). *Proc. R. Soc. Edinburgh*, **99**B(1/2), 83–103.

Nicholls, A., Sharp, K. A. & Honig, B. (1991). *Proteins*, **11**, 281–296.

Perrakis, A., Morris, R. & Lamzin, V. S. (1999). *Nature Struct. Biol.* **6**, 458–463.

Ramachandran, G. N., Kolaskar, A. S., Ramakrishnan, C., Sasisekharan, V. (1974). *Biochem. Biophys. Acta*, **359**(2), 298–302.

Read, R. J. (1986). *Acta Cryst.* A**42**, 140–149.

Rees, B. & Bilwes, A. (1993). *Chem. Res. Toxicol.* **6**(4), 385–406.

Rees, B., Bilwes, A., Samama, J. P. & Moras, D. (1990). *J. Mol. Biol.* **214**, 281–297.

Schneider, T. R., Kärcher, J., Pohl, E., Lubini, P. & Sheldrick, G. M. (2000). *Acta Cryst.* D**56**, 705–713.

Sheldrick, G. M. (1998). *Direct Methods for Solving Macromolecular Structures*, edited by S. Fortier, pp. 401–441. Dordrecht: Kluwer Academic Publishers.

Sheldrick, G. M. & Gould, R. O. (1995). *Acta Cryst.* B**51**, 423–431.

Sheldrick, G. M. & Schneider, T. (1997). *Methods Enzymol.* **277**, 319–343.

Smith, J. L., Corfield, P. W. R., Hendrickson, W. A. & Low, B. W. (1988). *Acta Cryst.* A**44**(3), 357–368.

Sutcliffe, M. J., Jaseja, M., Hyde, E. I., Lu, X. & Williams, J. A. (1994). *Nature Struct. Biol.* **1**(11), 802–807.

Usón, I. & Sheldrick, G. M. (1999). *Curr. Opin. Struct. Biol.* **9**, 643–648.

Usón, I., Sheldrick, G. M., de La Fortelle, E., Bricogne, G., Di Marco, S., Priestle, J. P., Grütter, M. G. & Mittl, P. R. E. (1999). *Structure*, **7**, 55–63.

Weeks, C. M., DeTitta, G. T., Hauptman, H. A., Thuman, P. & Miller, R. (1994). *Acta Cryst.* A**50**, 210–220.

Weeks, C. M. & Miller, R. (1999). *J. Appl. Cryst.* **32**, 120–124.

Acta Crystallographica Section D
Biological Crystallography
ISSN 0907-4449

addenda and errata

The atomic resolution structure of bucandin, a novel toxin isolated from the Malayan krait, determined by direct methods. Erratum

Peter Kuhn,[a] Ashley M. Deacon,[a] Doina-Silviana Comsa,[b] G. Rajaseger,[c] R. Manjunatha Kini,[c] Isabel Usón[d] and Prasanna R. Kolatkar[b]*

[a]Stanford Synchrotron Radiation Laboratory, SLAC, PO Box 4349, MS69, Stanford University, Stanford, CA 94309, USA, [b]Institute of Molecular and Cell Biology–Bioinformatics Centre, 30 Medical Drive, Singapore 117609, Singapore, [c]Bioscience Centre, Faculty of Science, NUS, Singapore 119260, Singapore, and [d]Institute of Inorganic Chemistry, Tammannstrasse 4, 37077 Göttingen, Germany

In the paper by Kuhn *et al.* [*Acta Cryst.* (2000), D**56**, 1401–1407] the name of the third author was given incorrectly. The correct name should be Doina-Silviana Comsa as given above.